ARTICLE

https://doi.org/10.1038/s41586-019-0911-2

Convergent estimates of marine nitrogen fixation

Wei-Lei Wang[1], J. Keith Moore[1], Adam C. Martiny[1,2] & François W. Primeau[1]*

Uncertainty in the global patterns of marine nitrogen fixation limits our understanding of the response of the ocean's nitrogen and carbon cycles to environmental change. The geographical distribution of and ecological controls on nitrogen fixation are difficult to constrain with limited in situ measurements. Here we present convergent estimates of nitrogen fixation from an inverse biogeochemical and a prognostic ocean model. Our results demonstrate strong spatial variability in the nitrogen-to-phosphorus ratio of exported organic matter that greatly increases the global nitrogen-fixation rate (because phytoplankton manage with less phosphorus when it is in short supply). We find that the input of newly fixed nitrogen from microbial fixation and external inputs (atmospheric deposition and river fluxes) accounts for up to 50 per cent of carbon export in subtropical gyres. We also find that nitrogen fixation and denitrification are spatially decoupled but that nevertheless nitrogen sources and sinks appear to be balanced over the past few decades. Moreover, we propose a role for top-down zooplankton grazing control in shaping the global patterns of nitrogen fixation. Our findings suggest that biological carbon export in the ocean is higher than expected and that stabilizing nitrogen-cycle feedbacks are weaker than previously thought.

Great uncertainty in global patterns of marine nitrogen fixation limits our ability to build mechanistic models that reliably predict the response of the ocean's nitrogen and carbon cycles to environmental change. Field N_2-fixation measurements are challenging to scale up because they have poor spatial coverage with high spatio-temporal variability, spanning six orders of magnitude[1–4]. Estimates from geochemical inverse models can use the more abundant hydrographic nitrate and phosphate concentration measurements to infer global rates of N_2 fixation. However, the existing P^* method[5–7] predicts a geographical distribution that conflicts with in situ measurements and prognostic biogeochemistry models. For example, in situ measurements in the tropical Pacific Ocean yield rates that are high in the west and low in the east but the P^* method predicts the opposite pattern[8,9]. On larger scales, observations and models suggest relatively high rates of tropical Atlantic N_2 fixation, whereas the P^* method predicts relatively low rates[4,7,10,11].

The P^* method attempts to diagnose N_2-fixation rates using a tracer, $P^* \equiv [PO_4^{3-}] - [NO_3^-]/16$, from observed surface phosphate and nitrate concentrations and its computed divergence using an ocean general circulation model. Assuming that non-diazotrophic production follows a constant N:P ratio of 16:1, P^* is unaffected by biological production so that any P^* divergences indicate the addition of newly fixed N.

Errors in the computed P^* divergence—due either to circulation or to the nutrient data— could explain the conflicting estimates. Coarse-resolution ocean general circulation models have non-negligible biases, and P^*, being computed as a concentration difference, tends to have larger relative errors than either $[PO_4^{3-}]$ or $[NO_3^-]$ alone. Furthermore, the low nitrate and phosphate concentrations in oligotrophic surface waters are often below the detection limits of traditional measurement techniques.

Another source of error is the assumption that organic matter produced by non-diazotrophic plankton follows fixed Redfield (16N:1P) stoichiometry. Although the P^* N_2-fixation estimate accounted for preferential remineralization of dissolved organic phosphorus (DOP) compared to dissolved organic nitrogen (DON), it did not consider the large-scale stoichiometric diversity of phytoplankton[7]. The impact of non-Redfield plankton cycling could be important. Model studies show that it greatly changes the amount of N_2 fixation necessary to explain observed P^* patterns while also modifying the size of the marine nitrogen reservoir[12–14] with similar impacts from non-Redfield cycling of DON and DOP[10,11]. Given recently documented C:N:P variations in particulate and dissolved organic matter as well as in the organic-matter export flux[15–19], it is important to construct models that do not assume constant stoichiometry.

Our global inversion diagnoses N_2 fixation by tracking the circulation of N and P separately through their organic and inorganic forms without assuming a constant N:P ratio in plankton or exported organic matter. It is based on a data-constrained circulation model[20,21] to minimize prognostic-model biases and uses the full water-column nitrate and phosphate measurements[22] to reduce the sensitivity to larger surface-water P^* errors.

We present data-constrained estimates of (1) the spatially variable N:P ratio of exported organic matter, (2) global patterns of N_2 fixation and denitrification, (3) the fraction of export production supported by newly fixed nitrogen, and (4) the degree to which N sources and sinks balance in recent decades. By construction, the inverse model is agnostic to the biological underpinnings that control N_2 fixation. To identify the mechanisms driving the inferred N_2-fixation patterns, we compare the inverse model results with results from the Community Earth System Model (CESM) ocean component, also modified to allow for variable N:P in phytoplankton and sinking organic matter, building on the non-Redfield treatment of dissolved organic matter (DOM)[11,17]. CESM produces a geographical distribution of N_2 fixation that is remarkably similar to the one inferred from the inverse model, and provides insights into the geochemical and ecological constraints on diazotrophs that drive global N_2-fixation patterns.

[1]Department of Earth System Science, University of California Irvine, Irvine, CA, USA. [2]Department of Ecology and Evolutionary Biology, University of California Irvine, Irvine, CA, USA.
*e-mail: fprimeau@uci.edu

Nitrogen fluxes and transformations

The inverse model is based on a system of conservation equations relating rates of losses of fixed N due to denitrification and anammox (bacterial anaerobic ammonium oxidation), physical transport due to circulation and gravitational settling of particles, biogeochemical transformations of N and P between organic and inorganic forms and between dissolved and particulate phases, and external inputs of fixed N (Fig. 1). The solution of these equations yields six state variables, which are the concentrations of dissolved inorganic nitrogen and phosphorus ([DIN] and [DIP]), and the dissolved and particulate phases of organic nitrogen and phosphorus ([DON], [DOP], [PON] and [POP]). The biogeochemical transformation rates are parameterized using only 13 parameters (Supplementary Table 1), which are constrained by a hydrographic database of [DIN], [DIP] and [DON][17,22] (see Supplementary Information and Supplementary Fig. 1). The fluxes and transformations inferred by the model are estimated under the assumption that the marine N cycle is in steady state and therefore balanced. We relax this assumption in the uncertainty analysis (see Methods).

N:P ratio of exported organic matter

The inversion yields a molar N:P ratio for the combined export from particulate and dissolved organic matter, denoted $(N:P)_{exp}$, ranging from more than 26:1 in the most nutrient-depleted gyres to less than 12:1 in nutrient-rich upwelling regions (Fig. 2a). We find a close correspondence between the inferred $(N:P)_{exp}$ and the N:P ratios measured in suspended particles[18,19,23] (Fig. 2b), similar to previous results examining C:P ratios[16]. This agreement suggests that at least part of the variance in the relative export of N compared to P originates in the stoichiometric diversity of plankton, rather than being entirely due to differential N and P remineralization[11,24]. We do find evidence for the preferential remineralization of P. The optimal parameter estimates indicate a shallower dissolution of POP compared to PON and a faster degradation of DOP compared to DON (see the optimal values of the power-law exponents controlling the vertical attenuation of the fluxes due to sinking POP and PON, b_P and b_N, and the remineralization rate constants for DOP and DON, κ_{dP} and κ_{dN}, in Supplementary Table 1).

The globally integrated ratio of biological export of N and P is 17.3:1, above the Redfield value of 16:1. The ratio is smaller than a simple averaging of the regional ratios shown in Fig. 2a would suggest, owing to the unequal regional contributions to total export. The elevated N:P ratios in the subtropical gyres are similar to those assumed in previous studies[12,13] but our estimates for the non-gyre regions are considerably higher, with mean ratios only modestly below Redfield. A global N:P export ratio of 17.3:1 is also much higher than the ratio of the oceanic reservoir of nitrogen and phosphorus[13], which is 14.3:1. Although it can be argued that the difference between these two ratios is a signature of denitrification, this is only partly true. In the presence of spatially varying N:P ratios, the average residence time of remineralized N need not equal that of P because of regional differences in the time for respired products to return to the surface[25,26].

Geographical distribution of N_2 fixation

The inversion reveals high N_2-fixation rates in the subtropical gyres where surface nutrients are depleted (and export N:P ratios are high) and low fixation rates in upwelling regions where surface macro nutrients are abundant (Fig. 3a and Supplementary Fig. 6). The most intense N_2-fixation rates are found downstream of the low-latitude upwelling regions in all basins. This pattern differs from the P^* estimate[7], which predicts the highest fixation rates in the eastern tropical Pacific upwelling regions and relatively low rates in the Atlantic Ocean.

Our global inversion is in good agreement with regional inversions for the Atlantic derived from isotope budgets[27]. For the overlapping regions northward of 24° N, 11° S, and 30° S we estimate N_2-fixation rates of $4.5^{7.0}_{3.1}$ teragrams of N per year (Tg N yr^{-1}), $27.9^{38.1}_{21.3}$ Tg N yr^{-1} and $36.2^{50.9}_{26.9}$ Tg N yr^{-1} respectively, whereas a previous study[27] estimated 3.0 ± 0.5 Tg N yr^{-1}, 27.1 ± 4.3 Tg N yr^{-1} and 30.5 ± 4.9 Tg N yr^{-1}, respectively.

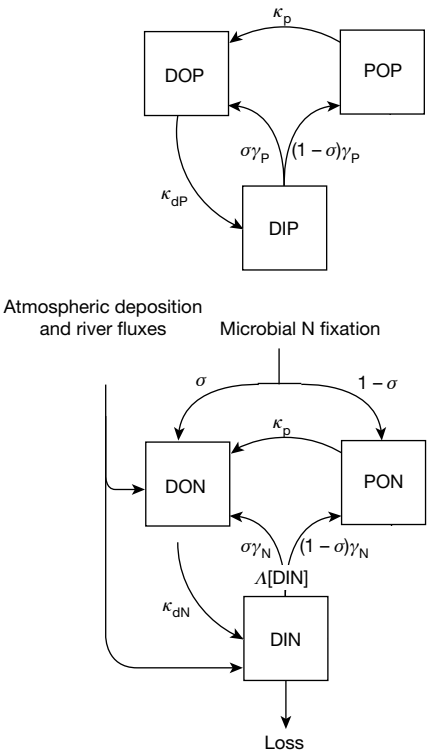

Fig. 1 | Schematic representation of the P-cycle and N-cycle models. Top, P cycle; bottom, N cycle. The dissolved tracers inorganic and inorganic phosphorus, DIP, DOP, and inorganic and organic nitrogen, DIN and DON are affected by advection and diffusion, whereas the particulate tracers, organic phosphorus and nitrogen, POP and PON are affected by gravitational settling. See Methods and Supplementary Information for the detailed mathematical formulation of the model and Bayesian inversion procedure. κ_p denotes the dissolution rate constant for particulate organic matter, κ_{dP} and κ_{dN} denote the remineralization rate constants for DOP and DON, γ_P and γ_N denote the local rate constants for the biological uptake of DIP or DIN, and σ is the fraction of the biological production allocated to the dissolved phase. The term Λ[DIN] limits the drawdown of DIN to prevent its concentration from becoming negative. The rate of nitrogen fixation is then diagnosed from the difference between the rate of production of organic nitrogen (DON + PON) and the rate of drawdown of DIN.

Our inversion generally supports the idea that little N_2 fixation occurs at temperatures below[28] 20 °C. The one exception to this is elevated N_2 fixation in the Arctic Ocean, where detectable N_2-fixation rates have been measured[29]. Our inverse estimates in this region must be interpreted with caution because the data constraining the circulation and nutrient-cycling are sparse (Supplementary Fig. 1).

Water-column losses are inferred to be highest in suboxic waters ($[O]_2 < 5$ mmol m^{-3}) flanking the Equator in the eastern tropical Pacific and in the northern Indian Ocean, where column-integrated rates can exceed 440 mmol m^{-2} yr^{-1} (Fig. 3c). The inferred water-column losses extend over the much larger volume of hypoxic waters ($[O]_2 < 60$ mmol m^{-3}) albeit at a lower rate, with non-negligible integrated water-column losses at oxygen concentrations above 20 mmol m^{-3} (Supplementary Fig. 7a, b), supporting the idea that substantial anaerobic respiration occurs within particle microenvironments in hypoxic waters[30] (but see also Supplementary Fig. 7c and d and Supplementary Figs. 14–16). Benthic losses are highest along continental margins, where more sinking organic matter reaches the bottom (Fig. 3d).

Our inversion reveals the importance of large-scale inter-basin transport of nitrogen for maintaining a globally balanced fixed-N budget (Table 1). The Atlantic Ocean, for example, maintains its balance by

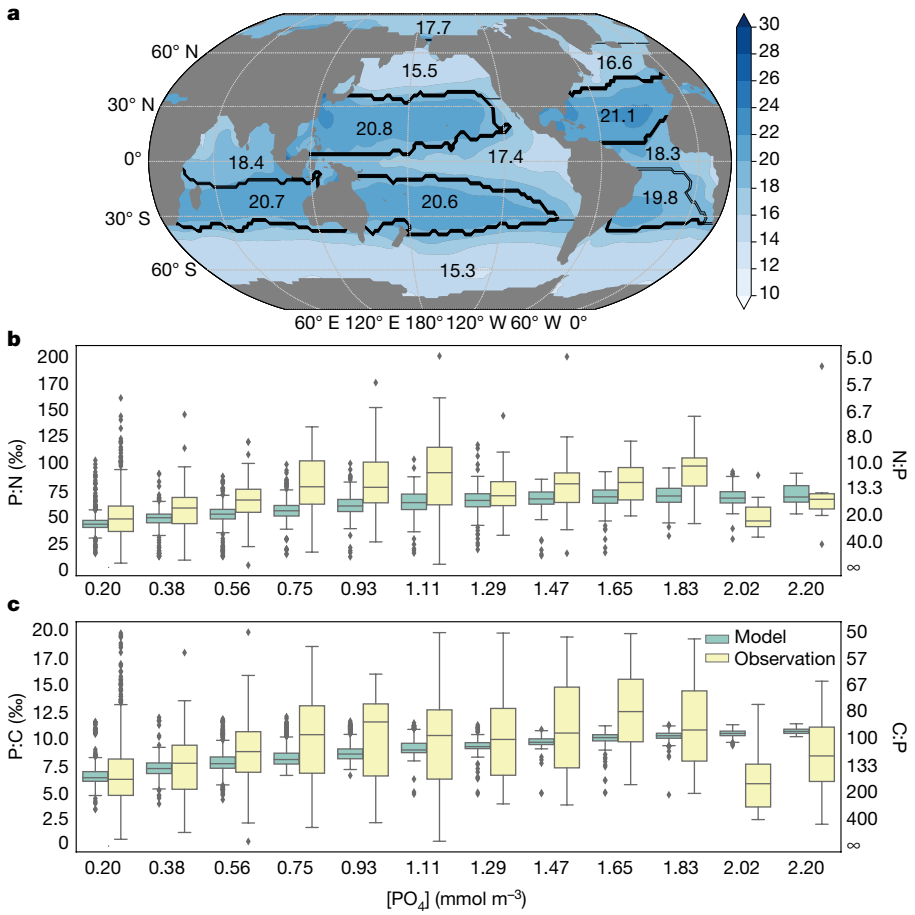

Fig. 2 | N:P ratio of exported organic material. a, Map of the N:P ratio of exported organic material ($(N:P)_{exp}$) inferred from the inverse model (colour scale). The numbers within the outlined regions correspond to the ratio of the integrated export of N to the integrated export of P for that region. **b**, Comparison of the measured N:P ratio in the stock of suspended particulate organic matter (POM) to that of the flux of exported organic matter inferred from the inverse model. **c**, Comparison of the measured C:P ratio in the stock of suspended POM to that in the flux of exported organic matter. For the calculation of the P:C export ratio a C:N ratio of 106:16 is assumed. The export flux includes the contributions from both sinking POM and the downward mixing of DOM and the box plot summarizes the distribution of all 2° × 2° grid boxes that fall into each phosphate concentration bin. The width of each bin is 0.18 mmol m^{-3}. The boxplots show the 25, 50 and 75 percentiles binned according to the phosphate concentration in the water. The whiskers cover 99.3 of the data with the remaining points shown as diamond symbols. Out of 1,774 POM data points 77 outliers are not shown, in order to keep the vertical axis to a reasonable range. Note that the left axes for panels **b** and **c** for the P:N and P:C ratios have a linear scale, whereas the right axes have a hyperbolic scale.

exporting about 15 Tg N yr^{-1} (33% of its N input). This result has been anticipated by prognostic model simulations and box-model budgets[31,32] and is consistent with strong evidence for P-limitation in the North Atlantic[33–35]. The Pacific Ocean supplies more than half of the fixed-N inputs, but also contributes disproportionately to losses because of intense water-column denitrification in the east Pacific low-oxygen zones, with a net basin-scale deficit of about 10 Tg N yr^{-1}, in agreement with a previous publication[31]. The Indian Ocean has a nearly balanced N budget (Table 1).

Microbial N_2 fixation supports more than 30% of the export production in all subtropical gyres and more than 50% in the North Pacific and South Atlantic (Fig. 4). These estimates are in agreement with independent budgets based on $\delta^{15}N$ measurements. At the Bermuda Atlantic Time-series Study (BATS) station in the subtropical Atlantic (32° 10′ N, 64° 30′ W), a $\delta^{15}N$ budget suggests that no input of newly fixed N is needed to close the N budget[36]—our inversion shows a negligible contribution of N_2 fixation. Similarly, a $\delta^{15}N$ budget for the Hawaii Ocean Time-series (HOT) (22° 45′ N, 158° 00′ W) suggests that 30% to 50% of export production is sustained[37] by newly fixed N—we estimate 30% to 40% (Fig. 4). Globally, we find that N_2 fixation supports about 8% of the global carbon export production, which is inferred by our inverse model to be approximately 12 petagrams of C per year.

Globally integrated marine N cycle budget

We estimate that N_2 fixation plus external inputs (Fig. 3b) delivers 200 Tg N yr^{-1} to the ocean. This input is balanced by water-column and benthic losses of 68 Tg N yr^{-1} and 132 Tg N yr^{-1} (Table 1).

The uncertainty for our global N_2-fixation rate estimate of 163 Tg N yr^{-1} is approximately 30% (Table 1). The globally integrated N_2-fixation and N-loss rates in our steady-state model can be scaled up or down with only modest changes in the spatial distribution of nutrients and N_2 fixation (Supplementary Figs. 12, 13). Thus, while the nutrient data provides strong constraints on the spatial pattern of N_2 fixation, it provides only weak bounds for the globally integrated rate. Our uncertainty estimate for the globally integrated rates therefore relies on ^{15}N isotopic constraints[38,39], which require a benthic to water-column loss ratio of between 1.3 and 3.0. This constraint means that we cannot scale the benthic-loss function up or down by more than 20% (Supplementary Table 2), leading to uncertainties of ±40% and ±12% for the globally integrated benthic and water-column loss rates (Table 1). In comparison, the uncertainty due to the other parameters is small, typically contributing relative errors of less than 2% in basin-integrated rates. External inputs due to rivers and atmospheric deposition are small in comparison to the sedimentary losses and therefore contribute relatively less uncertainty[31]. An alternative inversion based on pre-industrial atmospheric deposition[40] yields a

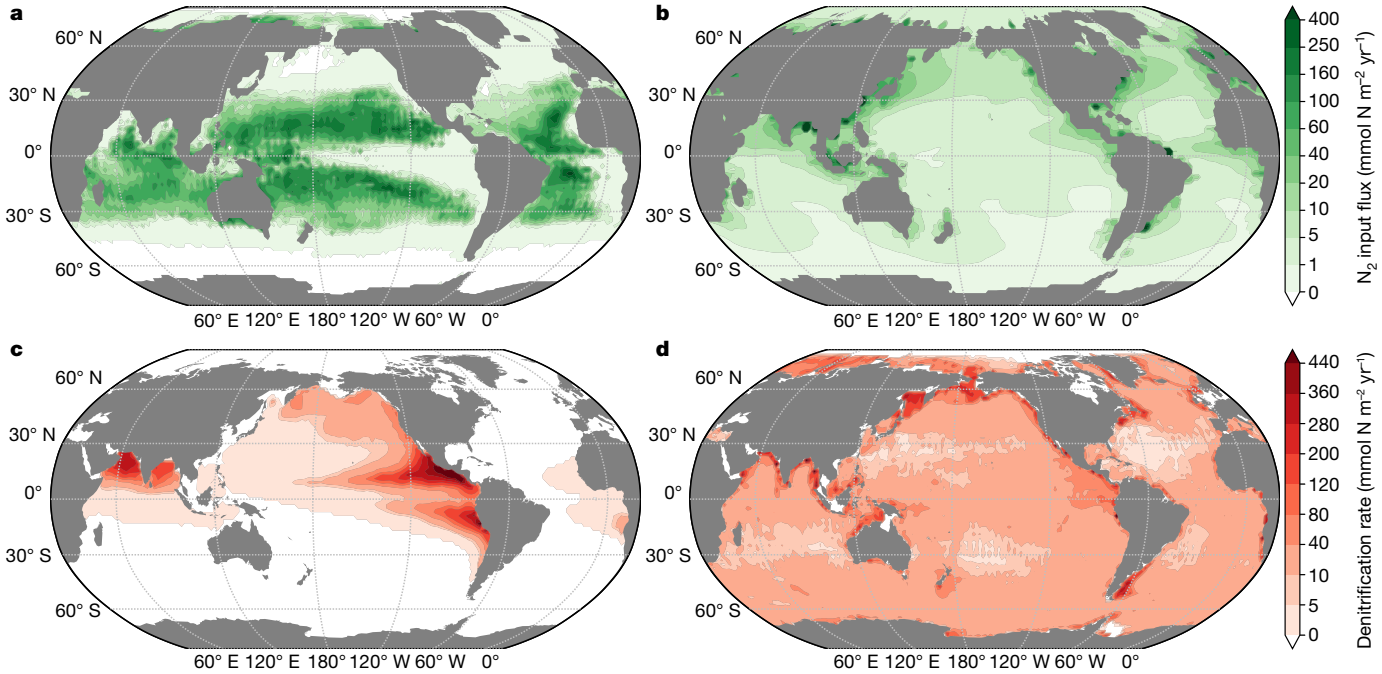

Fig. 3 | Maps of the column-integrated sources and sinks of fixed nitrogen. a, Input due to microbial N_2 fixation. **b**, Combined external input due to the present-day atmospheric deposition and river fluxes (see text). **c**, Loss due to water column denitrification and anammox. **d**, Loss due to sedimentary denitrification and anammox. Note that the colour scales are nonlinear in order to make the lower rates visible. (We note that whereas the spatial pattern of N_2 fixation is quite robust, the pattern of water-column denitrification is rather more uncertain. See Supplementary Information for alternative patterns of water-column denitrification that are also consistent with the DIN and DIP constraints.)

N_2-fixation rate that is about 10% higher than the one for present-day deposition (Supplementary Table 4), with only modest changes in the pattern of N_2 fixation (Supplementary Fig. 9). This approximately 10% decrease in N_2 fixation associated with increased atmospheric deposition is similar to what has been found in previous modelling studies, which found strong negative feedbacks limiting the impact of atmospheric deposition[41,42]. We do not explicitly estimate organic N burial in sediments, but this would be a similarly small fraction of our inferred benthic fixed N loss.

The uncertainty due to the relaxation of the steady-state assumption by allowing for slowly evolving nutrient fields (see Methods) has a modest impact on the parametric uncertainty. The most probable non-steady-state model has a global nitrogen budget, with a 1 Tg N yr^{-1} increment in the estimated benthic loss, an 11 Tg N yr^{-1} reduction in water-column denitrification, and a 16 Tg N yr^{-1} reduction in fixation, leaving a global source–sink imbalance of only 6 Tg N yr^{-1} (Table 1 and Supplementary Fig. 3). Because the inversion could have returned a much larger N-cycle imbalance, this suggests that our model is robust to undetected slowly evolving trends in the marine N cycle and that for recent decades there is no evidence for large imbalances on multidecadal timescales.

A potentially important source of uncertainty that we are unable to quantify in our annually averaged inverse model is the neglect of the seasonal cycle. However, because the model is constrained by data from the full water column, we expect that the muted seasonality at the base of the thermocline and deeper waters will anchor the inversion to produce the correct annually averaged fluxes. Further reductions in the uncertainty of the inverse estimates of N_2 fixation will require a seasonally varying circulation model that better resolves the coastal shelf regions and the oxygen minimum zones. Better data coverage in the Arctic would help to reduce large uncertainties in polar waters.

Ecological controls on N_2 fixation patterns

Our inverse model is largely agnostic about the biological underpinnings driving N_2 fixation. This is a positive feature as it reduces the chances that the answer is built into the model structure. To understand the mechanisms driving N_2-fixation patterns, we compare with biogeochemical simulations from the CESM ocean component, modified to allow for variable N:P ratios in phytoplankton and organic-matter export. The CESM-simulated N_2-fixation pattern is remarkably similar to the inverse-model estimate ($R^2 = 0.47$, see Figs. 3a, 5a). In both the prognostic and inverse models, N_2-fixation rates are suppressed directly

Table 1 | Biologically available nitrogen budget

	Input			Loss		
Basin	Atmospheric deposition	River input	Microbial N fixation	Water column	Sediment	Net
Pacific	12.0	3.3	$100.6^{132.8}_{78.9}$	$54.6^{58.1}_{42.7}$	$70.9^{106.6}_{48.2}$	$-9.7^{-9.2}_{-19.9}$
Atlantic	8.3	4.4	$34.0^{49.5}_{24.0}$	$0.3^{0.3}_{0.1}$	$31.0^{45.0}_{21.8}$	$15.3^{17.7}_{13.6}$
Indian	4.5	2.9	$26.6^{37.2}_{19.5}$	$13.8^{14.5}_{12.5}$	$22.8^{34.3}_{15.5}$	$-2.6^{-1.5}_{-3.3}$
Arctic	0.4	0.4	$1.8^{2.9}_{1.1}$	$0.0^{0.0}_{0.0}$	$5.8^{7.2}_{4.6}$	$-3.2^{-2.7}_{-3.9}$
Mediterranean	0.7	0.2	$0.2^{0.6}_{0.0}$	$0.0^{0.0}_{0.0}$	$0.9^{1.3}_{0.7}$	$0.2^{1.0}_{0.1}$
Global	25.8	11.2	$163.2^{222.9}_{125.6}$	$68.6^{72.9}_{55.8}$	$131.5^{194.5}_{90.7}$	$-5.7^{-0.4}_{-6.4}$

All numbers are in teragrams of N per year and correspond to the most probable value from the posterior probability distribution for the steady-state model. The only exception is the entry for the net global imbalance, which corresponds to the most probable value for the model in which we allowed for a slowly evolving disequilibrium. The upper and lower limits correspond to the upper and lower bounds obtained by combining inversions in which we relaxed the steady-state assumption to allow for a slowly decaying disequilibrium and inversions in which we scaled the rate coefficient for sedimentary denitrification by ±20%, which produced a sedimentary to water column denitrification ratio in the range of 1.3 to 3.0 in accord with the ^{15}N isotopic constraints.

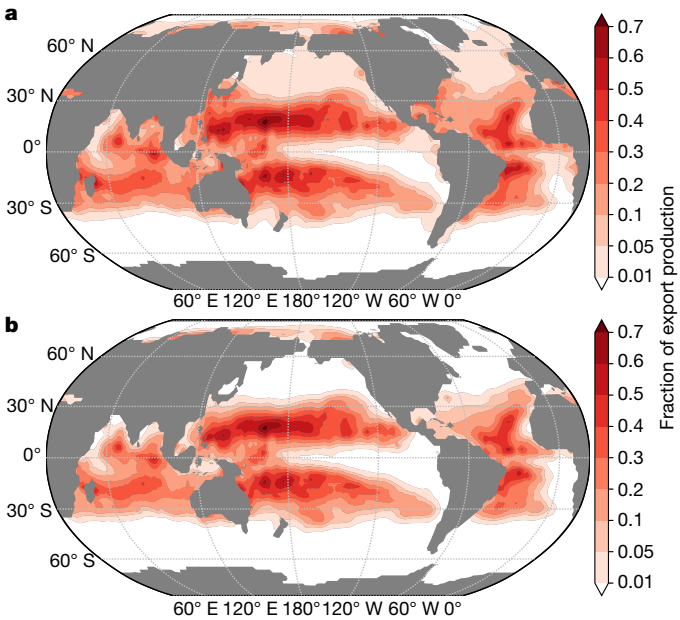

Fig. 4 | Contribution of newly fixed N to export production of carbon. **a**, Fraction of export production supported by the input of newly fixed N including microbial fixation, atmospheric deposition (present day), and river inputs. **b**, Fraction of export production supported by microbial N_2 fixation alone.

above the coastal and equatorial upwelling zones, with strong spatial decoupling of N_2 fixation and water-column denitrification associated with upwelling zones in the eastern tropical Pacific and Arabian Sea. Maximum N_2-fixation rates in both models are in downstream waters, advected away from the upwelling zones. The decoupling between upwelling zones and N_2 fixation occurs over much larger spatial scales in the Pacific, owing to iron-limitation in the offshore waters. N_2 fixation and the drawdown of 'excess' P are hampered by iron-limitation, pushing the highest N_2-fixation rates to the western tropical Pacific, where iron concentrations are higher, in line with field observations and previous modelling studies[11,32,43,44].

N_2-fixation patterns in CESM are driven by bottom-up limitations on diazotroph growth and top-down grazing by zooplankton. Previous studies have focused on bottom-up controls (the influence of nutrients, light and temperature) to explain global N_2-fixation patterns[11,13,14,43,44]. Diazotrophs need sufficient phosphorus and iron for growth, and benefit from competitors' N-limitation. In regions with high dust-input rates in the North Atlantic and northern Indian Ocean, diazotrophs tend to be phosphorus-limited, with iron availability constraining growth over much of the remaining low-latitude ocean (Fig. 5b).

Nutrient dynamics are important controls on diazotrophy, but we also suggest a key role for grazing, based on both first principles and the CESM results. Diazotroph growth rates are inherently slower than those of key microzooplankton grazers, which have growth rates similar to the fastest-growing phytoplankton[45,46]. This suggests that diazotrophs will always be in the density-dependent part of the grazing rate versus prey biomass curve, unlikely to escape grazing control and bloom. Furthermore, as diazotrophs typically account for only a small fraction of the phytoplankton community (in CESM up to about 10% of NPP in the most strongly N-limited regions and less than 3% in upwelling zones), it will be the growth of the more abundant and faster-growing, non-diazotrophic phytoplankton that determines zooplankton biomass, indirectly influencing the top-down grazing experienced by diazotrophs.

In CESM, diazotroph biomass is elevated and N_2-fixation rates are highest in the most N-limited regions where zooplankton biomass is low (Fig. 5a and Supplementary Fig. 21a). In the Indian basin, western Pacific, and coastal upwelling zones, diazotrophs are not strongly nutrient-limited (Fig. 5b). Top-down grazing pressure is keeping diazotroph biomass low, despite ambient nutrient concentrations that support near-maximal growth rates. The lowest diazotroph biomass is seen in the coastal upwelling zones, where other phytoplankton groups are blooming and zooplankton biomass is elevated (Supplementary Fig. 21a, c). A sensitivity experiment with the maximum grazing rate on diazotrophs reduced by a factor of 0.63 (giving them the same ratio of maximum grazing rate to maximum growth rate as diatoms) results in massive diazotroph blooms in the low-latitude coastal upwelling zones, boosting global N_2 fixation by 62% (Fig. 5c, Supplementary Fig. 21b, d and Supplementary Information). The high N_2-fixation rates in upwelling regions in this reduced-grazing simulation are similar to the P^* estimate. Thus, the CESM results suggest that grazing has a key role in the spatial decoupling of N_2 fixation and denitrification, and prevents the runaway denitrification losses that could occur with high N_2-fixation rates directly above the oxygen minimum zones[47]. These results are not dependent on the highly parameterized treatment of zooplankton and grazing in CESM, but should always arise in models that assume slower maximum growth rates for diazotrophic phytoplankton along with a grazing pressure similar to other phytoplankton.

Marine diazotrophs comprise a highly diverse group of organisms, but much of the pelagic N_2 fixation is thought to be by relatively slow-growing *Trichodesmium* spp. and small unicellular diazotrophs[46]. The top-down grazing argument is particularly applicable to unicellular diazotrophs, even if only a fraction of the microzooplankton community were to be preying on them. *Trichodesmium* spp. may have more specialized predators, but grows extremely slowly[46,48]. Copepods were recently shown to graze on all diazotroph types present in mesocosm experiments as primary or secondary consumers, with 28% of zooplankton N biomass coming from diazotrophy[49]. More studies of grazing impacts on plankton community composition and diazotrophy are needed.

Convergent estimates of N_2 fixation

Our results present convergent global estimates of marine N_2 fixation from two independent methods, an inverse model that infers N inputs from the observed nutrient concentrations and a prognostic Earth system model that explicitly resolves diazotrophic growth and N_2-fixation rates as a function of ambient nutrients, temperature and light, in the context of grazing and competition. The prognostic model provides plausible mechanistic controls that lead to the N_2-fixation pattern deduced by the inverse model. The export of excess fixed N from the Atlantic basin (about 15 Tg N yr^{-1}) shows that a substantial amount of N_2 fixation is geographically uncoupled from oxygen minimum zones, suggesting that some stabilizing nitrogen-cycle feedbacks might be weaker and slower than previously thought.

There is a strong similarity between the N:P of sinking organic matter inferred from the inverse model and simulated with CESM ($R^2 = 0.76$, Supplementary Fig. 19). Both models have elevated ratios in the subtropical gyres and N:P ratios only modestly below the Redfield value elsewhere. Prior studies have imposed much lower N:P ratios in the more productive regions[12,13]. To capture the higher N:P ratios observed in the gyres, N:P ratios in nutrient-rich regions had to be set very low to maintain an assumed 16:1 global mean for non-diazotrophs[13]. Our results suggest that the observed nutrient distributions are not compatible with a mean N:P ratio in organic matter export of 12:1 or lower in upwelling zones. Thus, given mean N:P export ratios in the gyres above 20:1, the global-mean N:P export ratio is greater than the Redfield value at 17.3:1 in our most-probable inverse estimate and 20.0:1 in CESM. The higher mean N:P ratio in sinking organic matter and excessively high water-column denitrification (134 Tg N yr^{-1}) in CESM relative to the inverse model leads to a higher total N_2 fixation of 238 Tg N yr^{-1}, with benthic denitrification losses of 160 Tg N yr^{-1} (Supplementary Fig. 17). The discrepancy is largely attributable to the coarse resolution in CESM, which does not capture the narrow, equatorial sub-surface jets critical for ventilating the oxygen minimum zones[50].

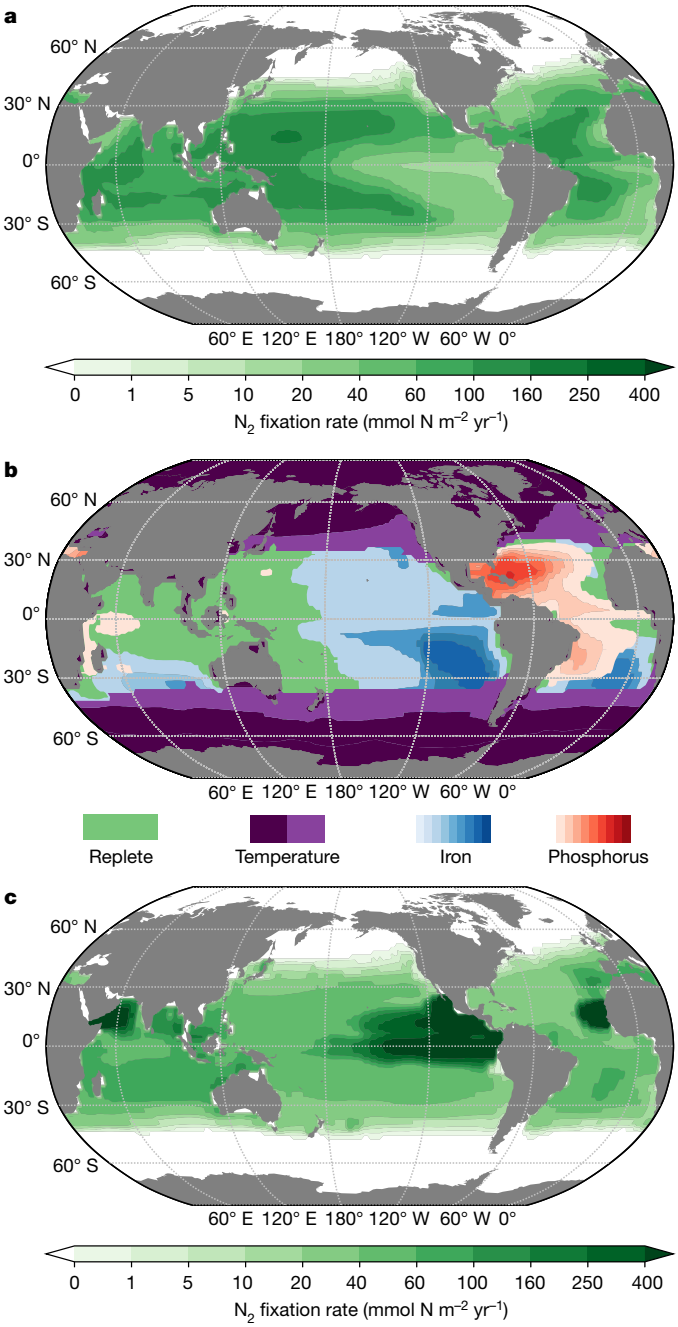

Fig. 5 | Prognostic model simulations of diazotrophs and N_2 fixation. **a**, Rates of N_2 fixation simulated by the CESM. **b**, Diazotroph growth limitation patterns. Nutrient 'replete' is where ambient nutrients could support growth at more than 90% of the maximum growth rate. **c**, Rates of N_2 fixation simulated by CESM with reduced grazing pressure, similar to that experienced by the diatoms (maximum grazing rate on diazotrophs reduced by a factor of 0.63).

Accounting for N:P variability in organic-matter export boosts global N_2 fixation, by 63% in the inverse model and by 50% in CESM, when compared to simulations with fixed Redfield stoichiometry (Supplementary Table 7 and Supplementary Figs. 10, 20). Spatially variable N:P ratios for plankton and exported organic matter allows global marine N-cycle models to be reconciled with ocean observations, and strongly affects the marine carbon cycle. Variable N:P ratios boost global POC export by 12% in CESM relative to the fixed Redfield simulation. Earth system models must include an explicit representation of this stoichiometric variability to capture the observed biogeochemical patterns and to accurately predict the response and feedbacks of ocean biogeochemistry to ongoing global warming.

Online content

Any methods, additional references, Nature Research reporting summaries, source data, statements of data availability and associated accession codes are available at https://doi.org/10.1038/s41586-019-0911-2.

Received: 31 March 2018; Accepted: 17 December 2018;
Published online 13 February 2019.

1. Mohr, W. et al. Methodological underestimation of oceanic nitrogen fixation rates. *PLoS ONE* **5**, e12583 (2010).
2. Großkopf, T. et al. Doubling of marine dinitrogen-fixation rates based on direct measurements. *Nature* **488**, 361–364 (2012).
3. Dabundo, R. et al. The contamination of commercial $^{15}N_2$ gas stocks with ^{15}N-labeled nitrate and ammonium and consequences for nitrogen fixation measurements. *PLoS ONE* **9**, e110335 (2014).
4. Luo, Y. W. et al. Data-based assessment of environmental controls on global marine nitrogen fixation. *Biogeosciences* **11**, 691–708 (2014).
5. Gruber, N. & Sarmiento, J. L. Global patterns of marine nitrogen fixation and denitrification. *Glob. Biogeochem. Cycles* **11**, 235–266 (1997).
6. Deutsch, C. et al. Denitrification and N_2 fixation in the Pacific Ocean. *Glob. Biogeochem. Cycles* **15**, 483–506 (2001).
7. Deutsch, C. et al. Spatial coupling of nitrogen inputs and losses in the ocean. *Nature* **445**, 163–167 (2007).
8. Knapp, A. N. et al. Low rates of nitrogen fixation in eastern tropical South Pacific surface waters. *Proc. Natl Acad. Sci. USA* **113**, 4398–4403 (2016).
9. Bonnet, S. et al. Hot spot of N_2 fixation in the western tropical South Pacific pleads for a spatial decoupling between N_2 fixation and denitrification. *Proc. Natl Acad. Sci. USA* **114**, E2800–E2801 (2017).
10. Somes, C. J. & Oschlies, A. On the influence of "non-Redfield" dissolved organic nutrient dynamics on the spatial distribution of N_2 fixation and the size of the marine fixed nitrogen inventory. *Glob. Biogeochem. Cycles* **29**, 973–993 (2015).
11. Letscher, R. T. & Moore, J. K. Preferential remineralization of dissolved organic phosphorus and non-Redfield DOM dynamics in the global ocean: impacts on marine productivity, nitrogen fixation, and carbon export. *Glob. Biogeochem. Cycles* **29**, 325–340 (2015).
12. Mills, M. M. & Arrigo, K. R. Magnitude of oceanic nitrogen fixation influenced by the nutrient uptake ratio of phytoplankton. *Nat. Geosci.* **3**, 412–416 (2010).
13. Weber, T. & Deutsch, C. Oceanic nitrogen reservoir regulated by plankton diversity and ocean circulation. *Nature* **489**, 419–422 (2012).
14. Landolfi, A. et al. A new perspective on environmental controls of marine nitrogen fixation. *Geophys. Res. Lett.* **42**, 4482–4489 (2015).
15. Weber, T. S. & Deutsch, C. Ocean nutrient ratios governed by plankton biogeography. *Nature* **467**, 550–554 (2010).
16. Teng, Y. C. et al. Global-scale variations of the ratios of carbon to phosphorus in exported marine organic matter. *Nat. Geosci.* **7**, 895–898 (2014).
17. Letscher, R. T. et al. Variable C:N:P stoichiometry of dissolved organic matter cycling in the Community Earth System Model. *Biogeosciences* **12**, 209–221 (2015).
18. Martiny, A. C. et al. Regional variation in the particulate organic carbon to nitrogen ratio in the surface ocean. *Glob. Biogeochem. Cycles* **27**, 723–731 (2013).
19. Martiny, A. C. et al. Strong latitudinal patterns in the elemental ratios of marine plankton and organic matter. *Nat. Geosci.* **6**, 279–283 (2013).
20. DeVries, T. & Primeau, F. W. Dynamically and observationally constrained estimates of water-mass distributions and ages in the global ocean. *J. Phys. Oceanogr.* **41**, 2381–2401 (2011).
21. Primeau, F. W., Holzer, M. & DeVries, T. Southern Ocean nutrient trapping and the efficiency of the biological pump. *J. Geophys. Res. Oceans* **118**, 2547–2564 (2013).
22. Garcia, H. E. et al. in *World Ocean Atlas 2013 Vol. 4 Dissolved Inorganic Nutrients (Phosphate, Nitrate, Silicate)* (eds Levitus, S. & Mishonov, A.) http://www.nodc.noaa.gov/OC5/indprod.html (NOAA Atlas NESDIS 76, US Government Printing Office, Washington DC, 2013).
23. Galbraith, E. D. & Martiny, A. C. A simple nutrient-dependence mechanism for predicting the stoichiometry of marine ecosystems. *Proc. Natl Acad. Sci. USA* **112**, 8199–8204 (2015).
24. Loh, A. N. & Bauer, J. E. Distribution, partitioning and fluxes of dissolved and particulate organic C, N and P in the eastern North Pacific and Southern Oceans. *Deep Sea Res. I* **47**, 2287–2316 (2000).
25. Primeau, F. W. & Holzer, M. The ocean's memory of the atmosphere: residence-time and ventilation-rate distributions of water masses. *J. Phys. Oceanogr.* **36**, 1439–1456 (2006).
26. DeVries, T., Primeau, F. & Deutsch, C. The sequestration efficiency of the biological pump. *Geophys. Res. Lett.* **39**, L13601 (2012).
27. Marconi, D. et al. Tropical dominance of N_2 fixation in the north Atlantic Ocean. *Glob. Biogeochem. Cycles* **31**, 1608–1623 (2017).
28. Tyrrell, T. The relative influences of nitrogen and phosphorus on oceanic primary production. *Nature* **400**, 525–531 (1999).
29. Blais, M. et al. Nitrogen fixation and identification of potential diazotrophs in the Canadian Arctic. *Glob. Biogeochem. Cycles* **26**, GB3022 (2012).
30. Bianchi, D. et al. Global niche of marine anaerobic metabolisms expanded by particle microenvironments. *Nat. Geosci.* **11**, 263–268 (2018).
31. Eugster, O. & Gruber, N. A probabilistic estimate of global marine N-fixation and denitrification. *Glob. Biogeochem. Cycles* **26**, GB4013 (2012).

32. Moore, J. K. & Doney, S. C. Iron availability limits the ocean nitrogen inventory stabilizing feedbacks between marine denitrification and nitrogen fixation. *Glob. Biogeochem. Cycles* **21**, GB2001 (2007).
33. Wu, J. F. et al. Phosphate depletion in the western North Atlantic. *Ocean Sci.* **289**, 759–762 (2000).
34. Sañudo-Wilhelmy, S. A. et al. Phosphorus limitation of nitrogen fixation by *Trichodesmium* in the central Atlantic Ocean. *Nature* **411**, 66–69 (2001).
35. Mills, M. M. et al. Iron and phosphorus co-limit nitrogen fixation in the eastern tropical North Atlantic. *Nature* **429**, 292–294 (2004).
36. Altabet, M. Variations in nitrogen isotopic composition between sinking and suspended particles: implications for nitrogen cycling and particle transformation in the open ocean. *Deep Sea Res. I* **35**, 535–554 (1988).
37. Karl, D. et al. The role of nitrogen fixation in biogeochemical cycling in the subtropical North Pacific Ocean. *Nature* **388**, 533–538 (1997).
38. Brandes, J. A. & Devol, A. H. A global marine-fixed nitrogen isotopic budget: implications for Holocene nitrogen cycling. *Glob. Biogeochem. Cycles* **16**, 67-1–67-14 (2002).
39. DeVries, T. et al. Marine denitrification rates determined from a global 3-D inverse model. *Biogeosciences* **10**, 2481–2496 (2013).
40. Lamarque, J.-F. et al. Historical (1850–2000) gridded anthropogenic and biomass burning emissions of reactive gases and aerosols: methodology and application. *Atmos. Chem. Phys.* **10**, 7017–7039 (2010).
41. Yang, S. & Gruber, N. The anthropogenic perturbation of the marine nitrogen cycle by atmospheric deposition: nitrogen cycle feedbacks and the ^{15}N Haber–Bosch effect. *Glob. Biogeochem. Cycles* **30**, 1418–1440 (2016).
42. Somes, C. J. et al. Limited impact of atmospheric nitrogen deposition on marine productivity due to biogeochemical feedbacks in a global ocean model. *Geophys. Res. Lett.* **43**, 4500–4509 (2016).
43. Somes, C. J., Schmittner, A. & Altabet, M. A. Nitrogen isotope simulations show the importance of atmospheric iron deposition for nitrogen fixation across the Pacific Ocean. *Geophys. Res. Lett.* **37**, L23605 (2010).
44. Ward, B. A. et al. Iron, phosphorus, and nitrogen supply ratios define the biogeography of nitrogen fixation. *Limnol. Oceanogr.* **58**, 2059–2075 (2013).
45. Edwards, K. F. et al. Light and growth in marine phytoplankton: allometric, taxonomic, and environmental variation. *Limnol. Oceanogr.* **60**, 540–552 (2015).
46. Fu, F.-X. et al. Differing responses of marine N_2 fixers to warming and consequences for future diazotroph community structure. *Aquat. Microb. Ecol.* **72**, 33–46 (2014).
47. Landolfi, A. et al. Overlooked runaway feedback in the marine nitrogen cycle: the vicious cycle. *Biogeosciences* **10**, 1351–1363 (2013).
48. O'Neil, J. M. & Roman, M. R. Ingestion of the cyanobacterium *Trichodesmium* spp. by pelagic harpacticoid copepods *Macrosetella*, *Miracia* and *Oculosetella*. *Hydrobiologia* **292/293**, 235–240 (1994).
49. Hunt, B. P. et al. Contribution and pathways of diazotroph-derived nitrogen to zooplankton during the VAHINE mesocosm experiment in the oligotrophic New Caledonia lagoon. *Biogeosciences* **13**, 3131–3145 (2016).
50. Getzlaff, J. & Dietze, H. Effects of increased isopycnal diffusivity mimicking the unresolved equatorial intermediate current system in an Earth system climate model. *Geophys. Res. Lett.* **40**, 2166–2170 (2013).

Acknowledgements This work was supported by the National Science Foundation (grant OCE 1436922 awarded to F.W.P.). F.W.P., J.K.M. and W.-L.W. also acknowledge support from the US Department of Energy Office of Biological and Environmental Research (grants DE-SC0007206, DE-SC0012550 and DE-SC0016539) and the RUBISCO-SFA (grant PC13115 to J.K.M.) and A.C.M. acknowledges financial support from the National Science Foundation (grants OCE-1046297 and OCE-1559002). We also acknowledge support from the National Science Foundation (grant OCE-1848576).

Reviewer information *Nature* thanks K. Casciotti, N. Gruber and C. Somes for their contribution to the peer review of this work.

Author contributions All authors contributed to the design of the study. W.-L.W. and F.W.P. built the inverse model and analysed its results. J.K.M. performed the CESM simulations and analysed its output. F.W.P., W.-L.W. and J.K.M. wrote the manuscript. All authors participated in the discussion of the results and commented on the manuscript.

Competing interests The authors declare no competing interests.

Additional information
Supplementary information is available for this paper at https://doi.org/10.1038/s41586-019-0911-2.
Reprints and permissions information is available at http://www.nature.com/reprints.
Correspondence and requests for materials should be addressed to F.W.P.
Publisher's note: Springer Nature remains neutral with regard to jurisdictional claims in published maps and institutional affiliations.

METHODS

Inverse model. *Ocean circulation.* The ocean circulation model used in this study was optimized using climatological observations of temperature, salinity, natural (pre-bomb) radiocarbon, sea surface height, phosphate, heat and freshwater fluxes, as well as the transient CFC-11 observations[20,21].

Biogeochemical fluxes and transformations. The biogeochemical conservation equations keep track of six nutrient pools, dissolved inorganic phosphorus and nitrogen (DIP and DIN), dissolved organic phosphorus and nitrogen (DOP and DON) and sinking particulate organic phosphorus and nitrogen (POP and PON).

The downward transport of P and N by the sinking and solubilization of POP and PON is treated in such a way as to produce power-law flux attenuation profiles, $(z/z_0)^{-b}$, with separate exponents b_P and b_N for P and N. The DOP and DON are respired back to DIP and DIN with separate rate constants κ_{dP} and κ_{dN}.

Biological production of organic phosphorus is modelled using a spatially variable uptake rate coefficient that is parameterized in terms of two adjustable parameters (α and β). Two additional parameters control the rate of dissolution of POP into DOP and the rate of DOP respiration (b_P and κ_{dP}). A dynamically variable N:P ratio, $r_{N:P}$, parameterized in terms of the local DIP concentration and two more adjustable parameters (A and B) relates the organic-phosphorus production to the organic-nitrogen production. As is the case for organic phosphorus, two adjustable parameters, b_N and κ_{dN}, control the rates of PON dissolution and DON respiration. We consider inputs of fixed N from N_2 fixation, atmospheric deposition, and rivers. Atmospheric and riverine inputs are prescribed[40,51] and the input of N_2 fixation is diagnosed from the model solution.

The net biological production of organic phosphorus in the euphotic zone is modelled using a spatially dependent uptake rate coefficient:

$$J_P = \gamma(\boldsymbol{r})[\mathrm{DIP}] \tag{1}$$

where $\gamma(\boldsymbol{r})$ is parameterized in terms of satellite-derived net primary production (NPP) and the observed phosphate concentration ($[\mathrm{DIP}]_{obs}$) using two adjustable parameters[16], α and β, that is:

$$\gamma(\boldsymbol{r}) = \begin{cases} \dfrac{\alpha\left(\frac{1}{r_{C:P}}\frac{\mathrm{NPP}(\boldsymbol{r})}{\mathrm{NPP}_0}\right)^{\beta}}{\frac{[\mathrm{DIP}]_{obs}(\boldsymbol{r})}{[\mathrm{DIP}]_0}} & \text{if } z < z_c \\ 0 \text{ otherwise} \end{cases} \tag{2}$$

In equation (2), $\boldsymbol{r}$ denotes the position on our model grid, $[\mathrm{DIP}]_{obs}$ is the objectively mapped phosphate concentration from the 2013 World Ocean Atlas and NPP is the satellite-derived carbon based net primary production (MODIS CbPM)[52,53], $r_{C:P} = 106$ for the Redfield model and $r_{C:P} = (c_1 + c_2[\mathrm{DIP}]_{obs})^{-1}$ with $c_1 = 0.006$ and $c_2 = 0.0069$ per mmol P per cubic metre for the variable stoichiometry model[23], z_c is euphotic zone depth, which is the depth of the upper two model layers (approximately the uppermost 73 m). To ensure that α has dimensions of inverse time NPP_0 is set to 1 mmol C m^{-2} s^{-1}. The full mathematical formulation of the P-cycle conservation equations are given in the Supplementary Information.

The net biological production of organic nitrogen is modelled using:

$$J_N = r_{N:P} J_P \tag{3}$$

with the N:P ratio parameterized in terms of the ambient DIP concentration according to:

$$r_{N:P} = A + B\Theta([DIP]; [DIP]_c, \Delta) \tag{4}$$

where A and B are adjustable parameters and where $[\mathrm{DIP}]_c = 0.075$ mmol m^{-3} and $\Delta = 1$ mmol m^{-3} are fixed parameters used to specify the limiter function:

$$\Theta(x; x_c, \lambda) \equiv \frac{1}{2}\left(1 - \tanh\left(\frac{x - x_c}{\lambda}\right)\right) \tag{5}$$

Sensitivity tests confirm that the inverse model solutions are not sensitive to $[\mathrm{DIP}]_c$ (Supplementary Information).

The water-column loss of fixed N is proportional to the rate of organic-carbon respiration, limited to regions where dissolved oxygen concentrations are sufficiently low. Two adjustable parameters, $[O_2]_c$ and Δ, control the shape of a limiter that ramps up the preference for nitrate over oxygen as the dominant oxidant. A third parameter k_w scales the overall reaction rate.

Benthic losses occur in the bottom grid cells of each water column. They are modelled following an empirical function[54]. We added a parameter s to scale the N-loss function, to account for uncertainties in this parameterization.

Owing to the loss of fixed N in low-oxygen environments, recycled and external N sources can support only a fraction of the biological production of organic N implied by the organic P production and local value of $r_{N:P}$. We therefore introduce a limiter that ramps down the uptake of DIN as its concentration approaches zero. The shape of this limiter is controlled by one last parameter, $[\mathrm{DIN}]_c$. Importantly, the limiter acts only on the drawdown of DIN and not on the production of newly fixed organic N. The difference between drawdown (uptake) and net production is the inferred rate of N_2 fixation, J_{fix}:

$$J_{fix} = \Theta([DIN]; [DIN]_c, \Gamma) J_N \tag{6}$$

The full conservation equations are given in the Supplementary Information.

The inversion process proceeds as follows. We use the model solution for the [DIN], [DIP] and [DON] state variables to define the mean of a joint probability function that we assign to the [DIN], [DIP] and [DON] observational data (see Supplementary Information). This probability function is conditioned on the model's parameters. We then use Bayes' rule to invert the probability function, to obtain the posterior probability for the unknown parameters conditioned on the known data. Finally, we draw samples from the posterior parameter distribution, which we then feed into the model equations to generate a probabilistic sample of the unobserved geochemical rates of interest. To make the computation feasible, we approximate the posterior probability for the parameters using a multivariate normal distribution. Because the normal approximation is poor for the benthic scaling parameters and the critical oxygen concentration, $[O_2]_c$, we separate the analysis into two levels of inference. At the first level, we find the conditional probability of the parameters conditioned on s and $[O_2]_c$. At the second level of inference, we vary s and $[O_2]_c$ and compare the relative posterior probability for these parameters after marginalizing out all of the other unknown parameters. Separating the analysis in this way has the advantage of making the parameter optimization more efficient and allows us to directly analyse the marginal sensitivity of our inferences to the overall benthic N loss rate and to the overall water-column N loss rates.

Even if we can neglect the uncertainty due to the missing seasonal cycle, there is still the possibility that the system is not in steady state. There is likely to be strong variability over shorter timescales affected by ENSO events and inter-annual variability in climate forcings[41]. Our inverse model results must therefore be viewed as a climatological estimate that averages over this type of variability. But there could also be weak longer-term trends in the nutrient fields that invalidate the steady-state assumption. To address this issue we augmented the model's list of adjustable parameters to include the amplitudes of the 263 eigenmodes of the linearized model that have e-folding decay timescales of 20 years or more (Supplementary Information). The long decay timescale of these modes would make them difficult to detect in a time series that is only a few decades long. Furthermore, because these modes are only weakly damped they are more likely to become excited by short-term variability[41]. We then jointly re-optimized the full list of parameters. The inclusion of the extra degrees of freedom had only a modest impact on the optimal values for most of the biogeochemical parameters. The only exceptions were for b_P, for which the value decreased by 16%, implying a deeper dissolution of POP, and κ_{dP}, for which the value increased fivefold, implying a very rapid remineralization of DOP. The impact on the inferred large-scale patterns of N_2 fixation due to these changes was small, as were the changes to the basin-wide budgets (Supplementary Table 3).

Prognostic CESM model simulations. The prognostic nitrogen cycle simulations were conducted using a modified version of the ocean component of CESM[55,56]. The model includes representations of four phytoplankton functional groups (diatoms, diazotrophs, calcifiers and smaller pico- to nanosized phytoplankton). The model also includes multiple potentially growth-limiting nutrients (nitrogen, phosphorus, iron and silicon). It has been well validated[55,56] and is often a component of CESM climate simulations[57,58]. The version of the model used here was modified to include variable plankton phosphorus cell quotas, in response to ambient phosphate concentrations after a previous publication[23], but with a minimum N:P ratio imposed, and to allow for variable N:P in the sinking particulate export. These modifications were included in CESM2. The CESM model results correspond to the average of the last 20 years of a 310-year simulation. More details are given in the Supplementary Methods.

Comparison of $(N:P)_{exp}$ to N:P of suspended POM. The particulate organic matter data used for the comparison between the N:P of suspended particulate organic matter with the inferred N:P of exported organic matter shown in Fig. 2 are from a previous publication[59].

Code availability. The code for the inverse model is available at DOI: 10.5281/zenodo.2020377. The optimized tracer transport operator used to run the inverse model is available upon request by contacting the corresponding author.

Data availability

All other data used to constrain the inverse model are publicly available (see Supplementary Information). The particulate organic matter data used for the comparison between the N:P of suspended particulate organic matter with the inferred N:P of exported organic matter shown in Fig. 2 is from a previous publication[59]. The model output for generating all of the other figures is available upon request.

51. Seitzinger, S. et al. Global river nutrient export: a scenario analysis of past and future trends. *Glob. Biogeochem. Cycles* **24**, GB0A08 (2010).
52. Westberry, T. et al. Carbon-based primary productivity modeling with vertically resolved photoacclimation. *Glob. Biogeochem. Cycles* **22**, GB2024 (2008).
53. *Ocean Productivity* http://www.science.oregonstate.edu/ocean.productivity/index.php (2008).
54. Bohlen, L., Dale, A. W. & Wallmann, K. Simple transfer functions for calculating benthic fixed nitrogen losses and C:N:P regeneration ratios in global biogeochemical models. *Glob. Biogeochem. Cycles* **26**, GB3029 (2012).
55. Moore, J. K., Doney, S. C. & Lindsay, K. Upper ocean ecosystem dynamics and iron cycling in a global three-dimensional model. *Glob. Biogeochem. Cycles* **18**, GB4028 (2004).
56. Moore, C. M. et al. Processes and patterns of oceanic nutrient limitation. *Nat. Geosci*. **6**, 701–710 (2013).
57. Moore, J. K. et al. Marine ecosystem dynamics and biogeochemical cycling in the Community Earth System Model [CESM1 (BGC)]: comparison of the 1990s with the 2090s under the RCP4. 5 and RCP8. 5 scenarios. *J. Clim*. **26**, 9291–9312 (2013).
58. Moore, J. K. et al. Sustained climate warming drives declining marine biological productivity. *Science* **359**, 1139–1143 (2018).
59. Martiny, A. C. et al. Concentrations and ratios of particulate organic carbon, nitrogen, and phosphorus in the global ocean. *Sci. Data* **1**, 140048 (2014).